Title

Extreme ultraviolet mask roughness effects in high numerical aperture lithography.

Journal

Applied Optics, 57(7)

ISSN

1559-128X

Authors

Naulleau, Patrick

Wang, Yow-Gwo

Pistor, Tom

Publication Date

2018-03-01

DOI

10.1364/ao.57.001724

Peer reviewed

Extreme ultraviolet mask roughness effects in high numerical aperture lithography

Patrick Naulleau, Yow-Gwo Wang, and Tom Pistor
Center for X-ray Optics, Lawrence Berkeley National Laboratory, Berkeley, California
EECS, University of California, Berkeley, California
Panoramic Technology Inc., Burlingame, California

Abstract
Given the reflective nature of extreme ultraviolet lithography and its extremely short operational wavelength, roughness of the optical surfaces is of significant concern. In particular, roughness in the mask multilayer leads to image plane speckle and ultimately patterned line-edge or line-width variability in the imaging process. Here we consider the implications of this effect for future high numerical aperture (NA) systems that are assumed to require anamorphic magnification projection optics. The results show significant anisotropic behavior at high NA as well as a substantial increase in relative patterned line variability in the shadowed direction when comparing 0.55 NA to 0.33 NA, despite the assumption of an anamorphic magnification system. The shadowed-direction patterned line variability is 2×2× larger than for unshadowed lines, and the majority of the increase in variability occurs in the low frequency regime.

1. INTRODUCTION
Photolithography is a cost-effective method of manufacturing integrated circuits. In this process, a circuit pattern master is first patterned onto a *mask*, and then an optical reduction system is used to replicate demagnified images of the mask onto a silicon wafer. The image projected to the wafer is recorded in a photosensitive film and ultimately etched into the silicon wafer. To continue the push to ever smaller feature sizes, the industry is now transitioning to extreme ultraviolet (EUV) lithography systems. EUV lithography, a short wavelength technique based on reflective optics and masks, is highly susceptible to roughness on these mirror surfaces. Roughness on the imaging mirrors used to project the demagnified image of the object (mask) to the image (wafer) plane leads to *flare*, which is essentially a broad halo around the image and simply reduces image contrast. When roughness is present on the reflective mask, however, it leads to a random phase term being added to the field reflected from the object. This random phase in the object plane in turn leads to image plane speckle and ultimately patterned line-edge or line-width variability in the imaging process. In lithography, this patterned line variability is typically referred to line-edge roughness (LER) and line-width roughness (LWR). LER is defined as the statistical deviation of the patterned edge from an ideal straight edge, and LWR is defined as the statistical deviation of the patterned line width as a function of position along the line. The impact of mask roughness on LWR near 0.3 numerical aperture (NA) is well documented in the literature; here we consider the implications for future high NA systems, which are also assumed to require anamorphic magnification projection optics to mitigate mask 3D effects.
Mask multilayer roughness contributes to patterning variability by way of the imaging process coupling phase roughness to speckle (random intensity fluctuations) in the aerial image, and ultimately variability in the printed pattern. Because EUV lithography relies on a reflective mask, it is particularly vulnerable to this effect compared to transmission deep ultraviolet (DUV) masks. In reflection, mask height variability is geometrically coupled to phase variability, scaled by a factor of 2 and thus, at the 13.5-nm EUV wavelength, very small levels of roughness will contribute to significant modulation of the phase. Although the lithographic process involves reimaging the mask surface to the wafer, to the extent the optical system cannot capture 100% of the scatter light, the process will remain sensitive to phase errors. Moreover, as defocus is introduced into the system, the imaging condition no longer strictly holds, and phase errors at the mask directly couple to intensity variation or speckle. The problem becomes increasingly severe as the illumination coherence is increased, something often done for resolution enhancement.

2. MODELING MASK MULTILAYER ROUGHNESS
In principle, the question of mask surface roughness coupling to LER can be understood analytically using partially coherent image formation theory coupled with the statistical representation of the mask as a random phase object; however, the problem quickly becomes intractable even under the small phase perturbation approximation. Simpler analytic geometric optics approaches describing the rough mask in terms of local slope error are also not suitable because they fail to account for the critical impact of partial coherence on the process. Moreover, the geometric analysis does not capture the fact that the extent to which speckle couples to pattern variability (edge displacement)

depends on the aerial-image intensity slope at the edge of the feature (dI/dxdI/dx), also known as the line-edge slope. Given a fixed speckle contrast, the edge movement is more severe with a smaller line-edge slope.
Given the difficulties above, numeric modeling of the partially coherent imaging process remains the most viable method for studying relevant cases of mask-roughness-induced variability. Rendering the problem numerically tractable, however, typically requires the problem to be reduced to two-dimensional instead of full three-dimensional modeling. The first step in the modeling is in the description of the roughness. EUV lithography masks utilize reflective coatings typically comprising 40 or more bilayers. If one starts with knowledge of the uncoated substrate surface, multilayer growth models can be used to predict the coating properties throughout the stack. From the calculated coating properties, rigorous electromagnetic field modeling could be used to calculate the electric field reflected from the mask. However, such an approach would be extremely computationally intensive.
In most cases relevant to the moderate roughness found on EUV masks, the effect of the rough mask can be readily modeled as a pure two-dimensional phase distribution. The validity of this simplified approach has previously been demonstrated by directly comparing the simplified approach to rigorous electromagnetic modeling of a full multilayer stack. In practice, this simplification works because the vast majority of the nonconformal multilayer growth occurs within a small number of layers closest to the substrate. Within the EUV penetration region near the top of the EUV multilayer, however, the layer growth tends to be conformal for the roughness range of interest here.
The typical method of determining the two-dimensional phase function is to measure the topographic profile of the mask using, for example, atomic force microscopy (AFM), and then computing the phase based on the geometric path-length differences imparted by assuming the EUV light to be reflected from the top surface of the mask. This method, however, tends to break down as mask qualities begin to approach the AFM noise floor, and/or the roughness spatial frequency bandwidth approaches the angular bandwidth limits of the Bragg coating. To get around this issue, we can instead use EUV scattering measurements to determine the effective EUV phase roughness.
Figure 1 shows the measured effective isotropic EUV roughness power spectral density (PSD) for a high-quality EUV mask. The green trace shows the raw PSD, and the blue trace shows a fractal fit with a correlation length of 37 nm and roughness exponent of 0.84. The root mean square (rms) roughness is 67 pm.

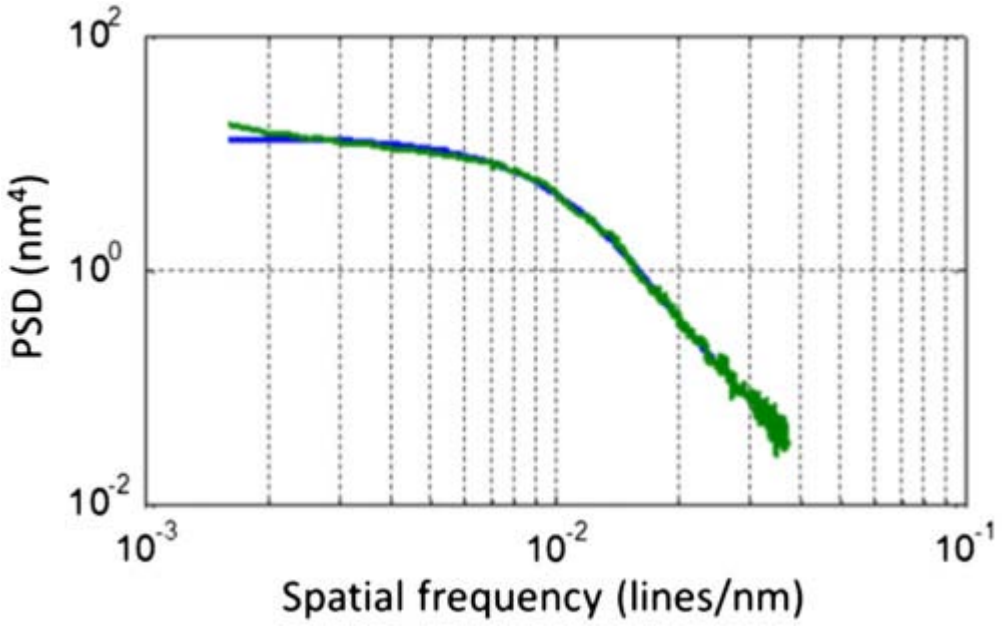

Fig. 1. Measured effective isotropic EUV roughness PSD for high-quality EUV mask. Green trace shows raw PSD and blue trace shows fractal fit. Correlation length=37 nmlength=37 nm; roughness exponent=0.84exponent=0.84; rms roughness=67 pmroughness=67 pm.

From this PSD, we can then synthesize an effective mask *transmittance function* for use in aerial image modeling. The first step is to create a random surface with roughness PSD matching the mask of interest, for example the PSD shown in Fig. **1**. As described above, we next convert this surface to a *transmittance function* by applying the so-called single surface approximation where the *transmittance function* amplitude is set to 1 and the phase is set to $4\pi h/\lambda 4\pi h/\lambda$, and where $h h$ is the surface height and $\lambda\lambda$ is the wavelength ($4\pi 4\pi$ comes from the fact that the mask is actually used in reflection). Figure **2** shows the phase of the *transmittance function* corresponding to the PSD shown in Fig. **1**.

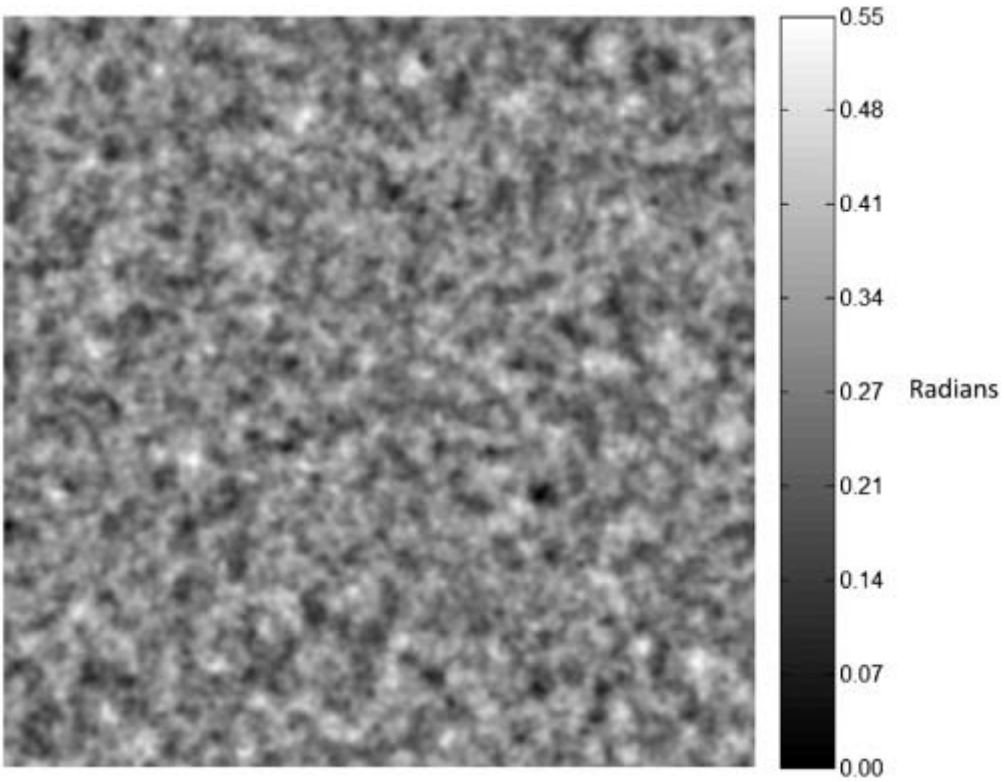

Fig. 2. Synthesized mask *transmission function* phase for a mask with the PSD shown in Fig. 1. Synthesized width on mask is 2 μm.

The synthesized clear area on the mask described above could then be used to model the aerial image speckle that impacts the LWR, but of more interest is to model LWR directly. To this end, we must add an absorber pattern to the mask. Accurately capturing the mask 3D effects in the absorber pattern, however, requires rigorous 3D modeling to be used for this step. The Hyperlith software package by Panoramic Inc. is used to compute the mask electric field for the absorber pattern, which is then coherently combined with the mask roughness electric field described above. This new combined electric field is then used as the input to the aerial image simulator capturing both mask absorber 3D effects and multilayer roughness effects. This hybrid method is much more computationally efficient then trying to perform rigorous electromagnetic modeling of the full large-area 3D mask, yet captures the key 3D effects in the absorber pattern. The improved computational efficiency comes from the fact that for performing the rigorous 3D modeling of the lines we need only model a cross-section of the lines and only over one period. The results can then be tiled to cover the total area we want to model the roughness effect over. Figure 3 shows the resulting electric field for shadowed 10-nm lines and spaces. Standard EUV absorber specifications are used and the absorber is assumed to have an ideal profile and no variability, thus no scatter. The line width on the mask is assumed to be 8×8× the line width on the wafer, as would be the case for a high NA anamorphic system, therefore the lines are 80 nm on the mask. Quasar dipole illumination with an inner sigma of 0.2, an outer sigma of 0.9, and an opening angle of 90 deg is assumed with a chief ray angle of incidence of 6 deg. Figure 4 shows an example resulting aerial image where the focus is set to a value of −40 nm−40 nm, or approximately $0.9\lambda/NA20.9\lambda/NA2$. The imaged lines and spaces are 10 nm, and the resulting aerial image LER and LWR is evident.

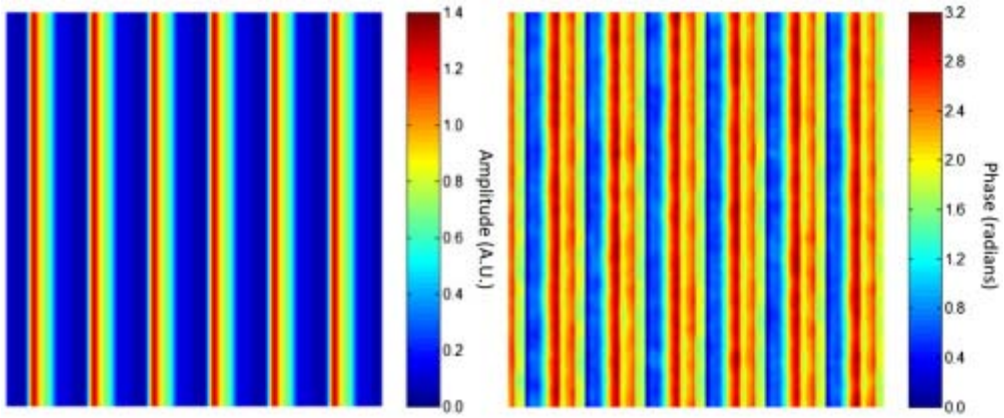

Fig. 3. Synthesized mask *transmission function* amplitude and phase for mask with the PSD shown in Fig. 1 and 10- nm (80 nm on the mask) shadowed lines and spaces. The depicted mask area width is 1 μm.

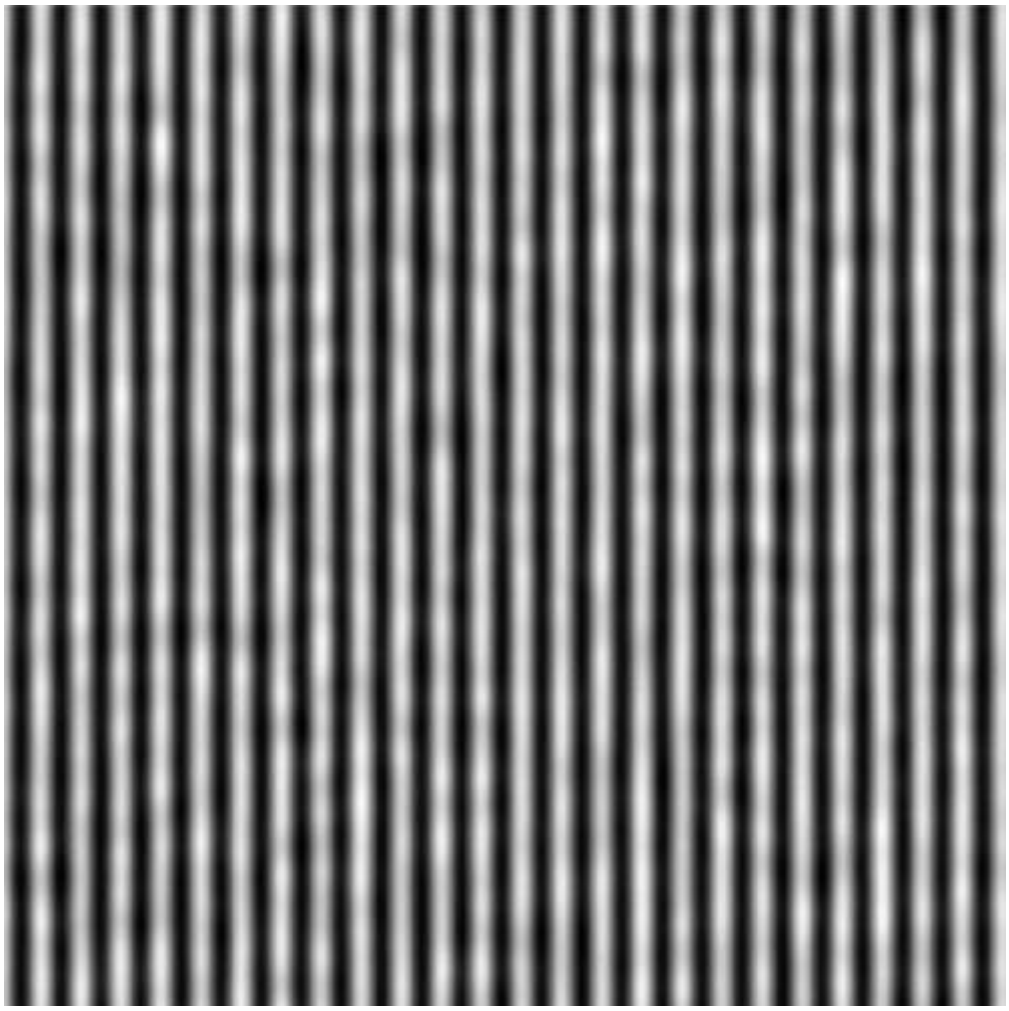

Fig. 4. Computed aerial image of 10-nm lines and spaces for anamorphic system in 8×8×(shadowed) direction at defocus value of 0.9λ/NA20.9λ/NA2. Depicted wafer plane aerial image size is 500 nm×500 nm500 nm×500 nm (4 μm×2 μm4 μm×2 μm on mask).

3. AERIAL IMAGE ANALYSIS RESULTS

In this section we present aerial image modeling results considering two different optical configurations: the reference case of 0.33 NA and the anamorphic case of 0.55 NA. Both horizontal (shadowed) and vertical (unshadowed) lines and spaces are studied, and in each case we use the modeling methods described above including the described Quasar dipole illumination settings. In the anamorphic case, the shadowed lines correspond to the 8×8×magnification direction and the unshadowed lines are imaged at 4×4×. At 0.33 NA, both directions are imaged at 4×4×. For the results below, we compute a total of 10 independent realizations of the random phase mask with a total simulated width of approximately 2 μm on the mask yielding a total length of simulated line ranging from approximately 220–460 μm depending on the optical configuration. Given an expected LWR correlation length in the 40–80-nm range in mask coordinates as determined by the resolution limit of the optic, the large values for the total simulated line length relative to the LWR correlation length ensure statistically meaningful results in the LWR analysis.

A. Reference Case: 0.33 NA

For reference, we begin with the conventional 0.33 NA case. Figure 5 shows the LER and LWR results for 16-nm vertical (unshadowed) lines and spaces through focus. The LER and LWR values were computed from the simulated aerial images using a commercially available software package. The focal range is set to approximately ±0.9λ/NA2±0.9λ/NA2. Identical results are seen for the left and right edges as a result of these being unshadowed lines and an aberration-free optical system being assumed. Comparing the average LER to the LWR, we find the LWR to be less than sqrt(2) times the LER indicating edge to edge correlation. This is a result of operating near the resolution limit of the optical system. At a defocus value of +0.6λ/NA2+0.6λ/NA2 the mask-roughness-induced LWR is ~0.4 nm~0.4 nm for the 67-pm roughness mask considered here. We note that these results can be extrapolated to a different level of mask phase roughness using linear scaling [**31**].

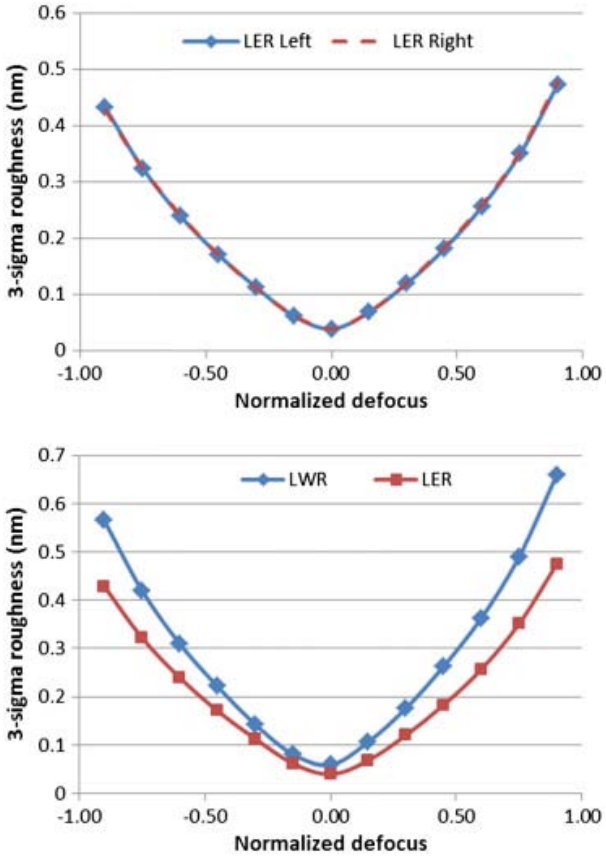

Fig. 5. Aerial image LER and LWR through focus for 16-nm unshadowed lines and space imaged at 0.33 NA. Defocus normalized to λ/NA2λ/NA2.

Turning next to horizontal (shadowed) 16-nm lines and spaces yields the results in Fig. 6. In this case we observe a difference in the LER performance on the two different sides of the line. We also see significant asymmetry through focus including varying divergence between the LWR and LER as well as increased variability values relative to the unshadowed lines.

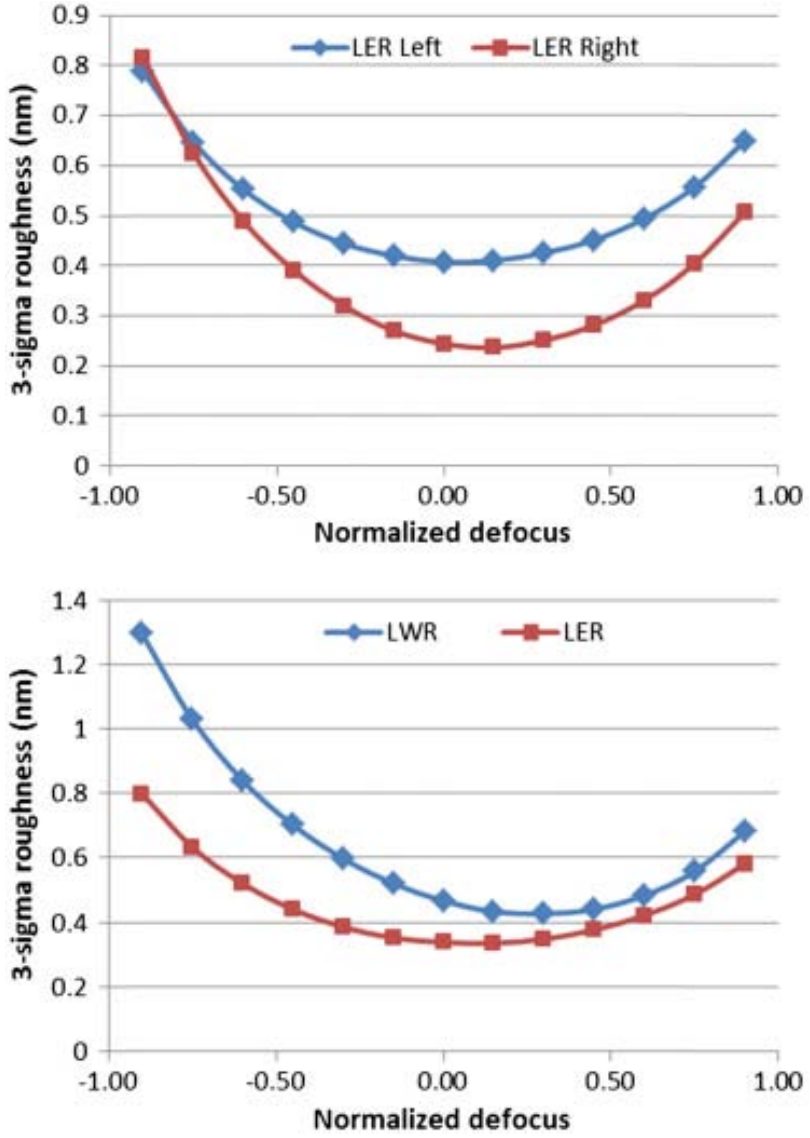

Fig. 6. Aerial image LER and LWR through focus for 16-nm shadowed lines and space imaged at 0.33 NA. Defocus normalized to λ/NA2λ/NA2.

Finally, we directly compare the shadowed and unshadowed feature LWR PSD at a defocus value of -0.6λ/NA2-0.6λ/NA2 (Fig. 7). As expected, the results show an identical cutoff frequency for LWR on the two different orientation lines. We also see that the elevated levels of LWR on the shadowed lines come primarily from the lower frequencies. Note that the detailed shape of the spectral response is focus-dependent as determined by the speckle transfer function of the optical system.

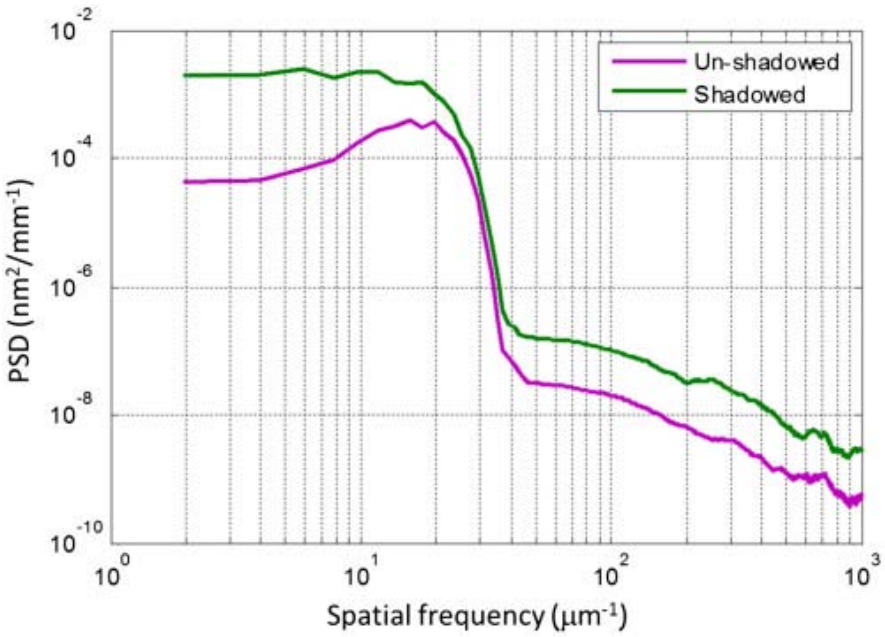

Fig. 7. LWR power spectral density (PSD) at defocus of −0.6λ/NA2−0.6λ/NA2.

B. Anamorphic High NA: 0.55 NA

In this section we consider the anamorphic 0.55 NA case with 10-nm lines and spaces. The 10-nm line width is chosen to nominally achieve the same feature size to NA ratio used in the 0.33 NA case. Figure 8 shows the results for the unshadowed (vertical) lines where we see similar behavior as for the 0.33-NA case.

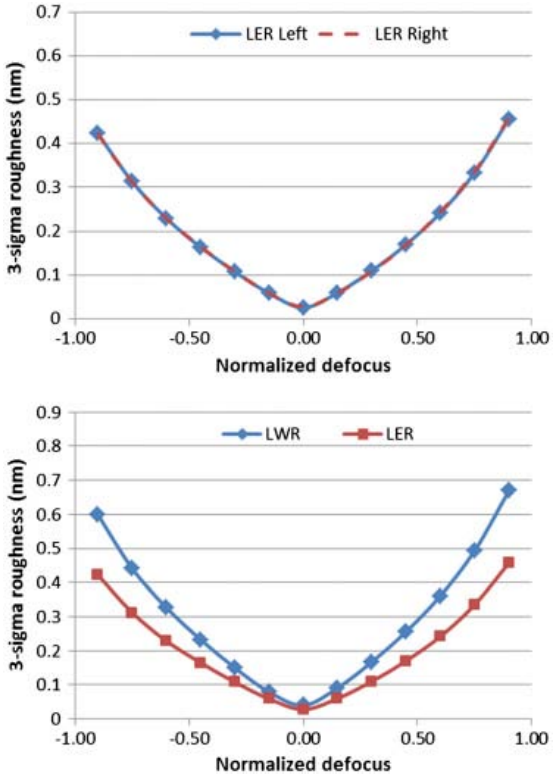

Fig. 8. Aerial image LER and LWR through focus for 10-nm unshadowed lines and spaces at 0.55 NA. Defocus normalized to λ/NA2λ/NA2.

Turning next to the shadowed (horizontal) lines (Fig. 9), we again see similar behavior as for the 0.33-NA case. Direct comparisons of the 0.33- and 0.55-NA cases show that in absolute terms the high NA case achieves essentially identical variability as does the 0.33-NA case. This is a result of operating at equivalent NA-normalized resolution and normalized defocus ranges and increasing the magnification in the shadowed direction for the high NA case thereby keeping the shadowing effects approximately the same in the two conditions. Because the NA-normalized imaging parameters are closely matched, we expect the image contrast to also be matched. Coupling this fact with the observation of nearly identical variability for the 0.33 and 0.55 NA cases indicates that the through-focus speckle contrast is also matched. This is expected since the speckle contrast depends on the normalized defocus rather than on the absolute defocus.

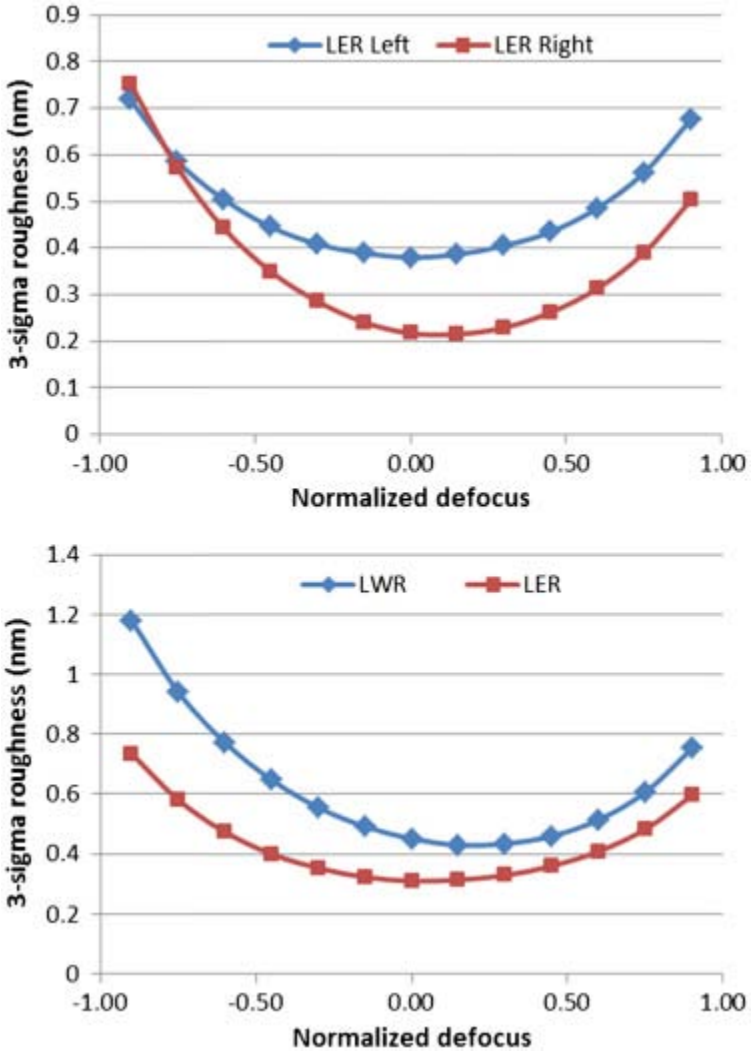

Fig. 9. Aerial image LER and LWR through focus for 10-nm shadowed lines and spaces imaged at 0.55 NA.

The LER and LWR comparisons above are in absolute numbers; however, it is arguably more relevant to consider fractional variability instead. In other words, the LER and LWR normalized by the nominal line width, which is 16 and 10 nm for the 0.33 and 0.55 NA cases, respectively. Such a comparison is shown in Figs. 10 and 11. For unshadowed lines (Fig. 10) we see the fractional LWR increase by approximately 70% at the edge of focus for 0.55

NA compared to 0.33 NA. The fractional LER increases by approximately 55%. Considering instead the shadowed lines (Fig. 11), we see a similar increase in fractional LER and LWR but throughout the normalized focus range instead of just at the edge of focus. The fractional LWR values at the edge of focus are found to exceed 10% in the 0.55 NA case. Achieving 0.55-NA performance equivalent to 0.33-NA performance in terms of fractional LWR would require the mask multilayer roughness to be improved by approximately 70%, i.e., reduced to better than 35 pm.

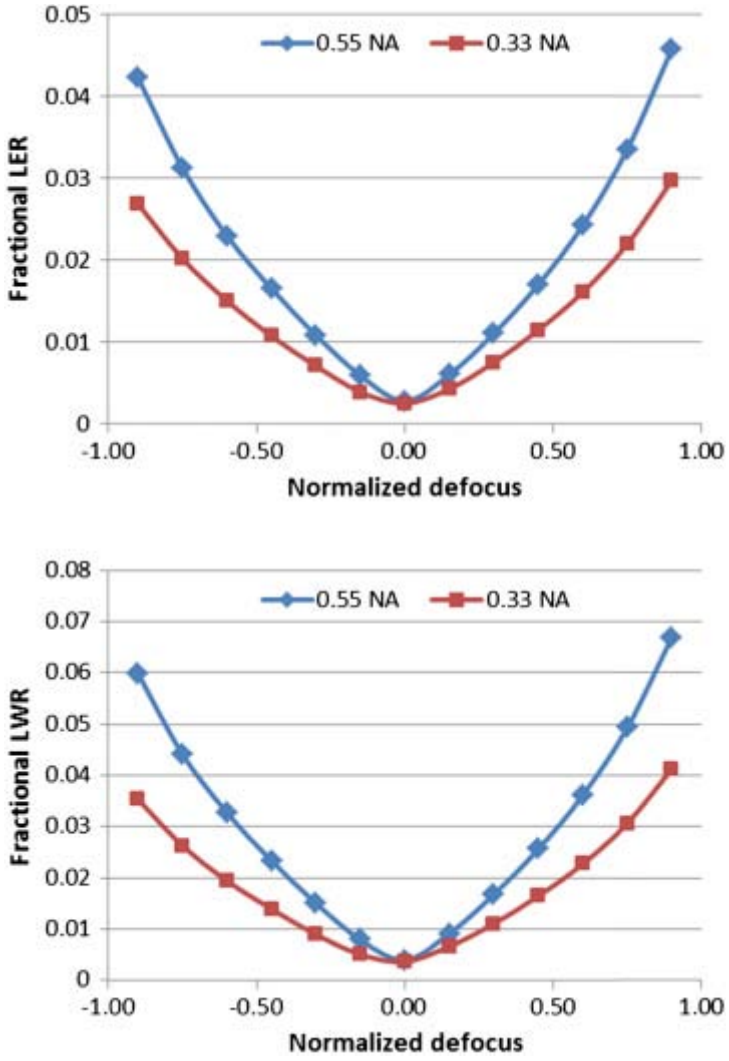

Fig. 10. Direct comparison of the unshadowed line-space aerial image fractional LER and LWR through focus for the 0.33 and 0.55 NA cases.

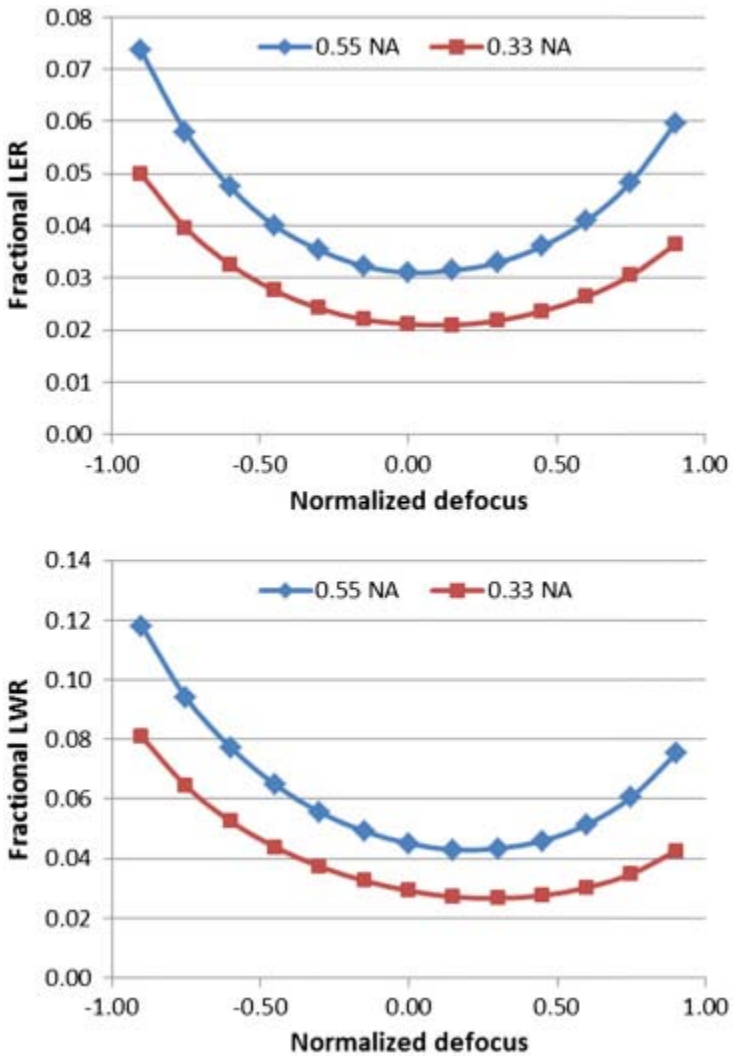

Fig. 11. Direct comparison of the shadowed line-space aerial image fractional LER and LWR through focus for the 0.33 and 0.55 NA cases.

Finally, we repeat the PSD analysis for the anamorphic case (Fig. 12). Despite anamorphic imaging of isotropic mask roughness, the frequency cutoff in the image plane remains isotropic since it is determined by the isotropic image side NA. The detailed spectral response, however, still exhibits similar anisotropic effects as seen for conventional 0.33 NA. Namely, we see anisotropy in the low frequency behavior (frequencies below 20/μm). Figures 13 and 14 show the through-focus behavior of the LWR PSD for shadowed and unshadowed lines, respectively. The spectral hump observed in the nonshadowed case with defocus can be attributed to the speckle transfer function [32], which is determined by the *sin* of the pupil phase function for defocus. In the shadowed case, the mask 3D effects lead to a more complicated effective aberration (or phase) function in the pupil, thus spreading out the spectral impact.

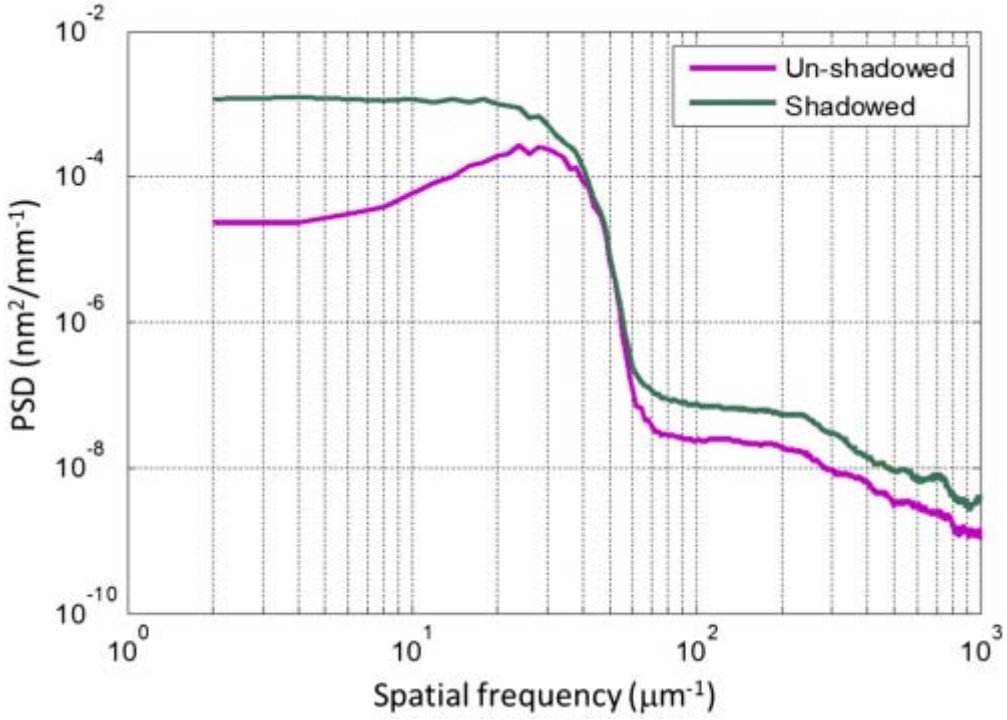

Fig. 12. LWR PSD for anamorphic case with 10-nm lines and spaces at defocus of −0.6λ/NA2−0.6λ/NA2.

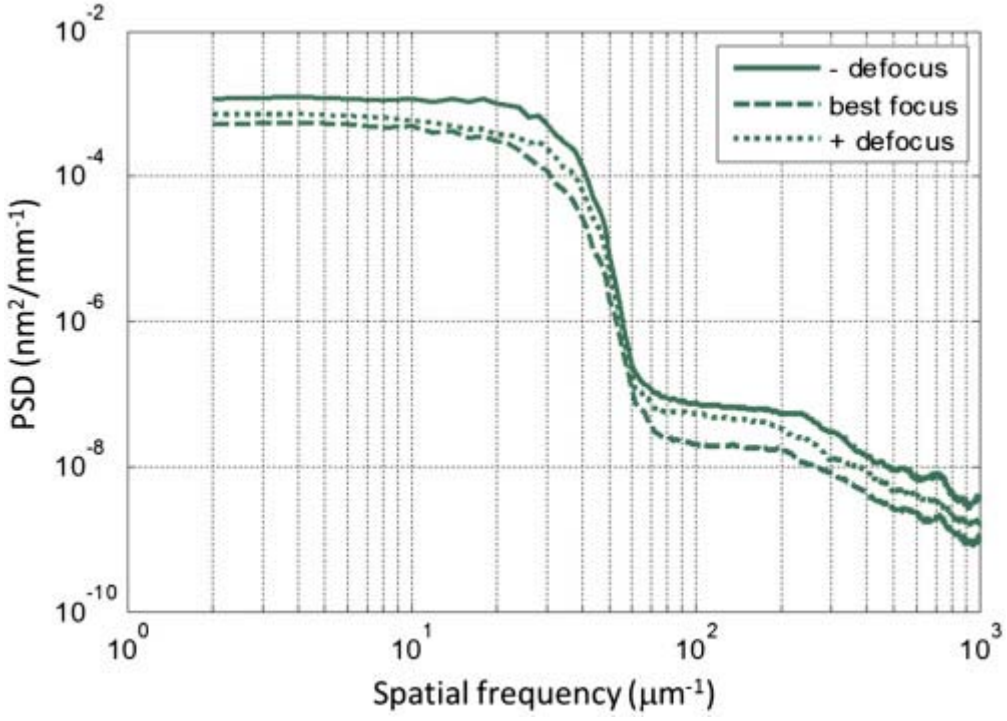

Fig. 13. LWR PSD for anamorphic case with 10-nm shadowed lines and spaces at defocus values of 0 and ±0.6λ/NA2±0.6λ/NA2.

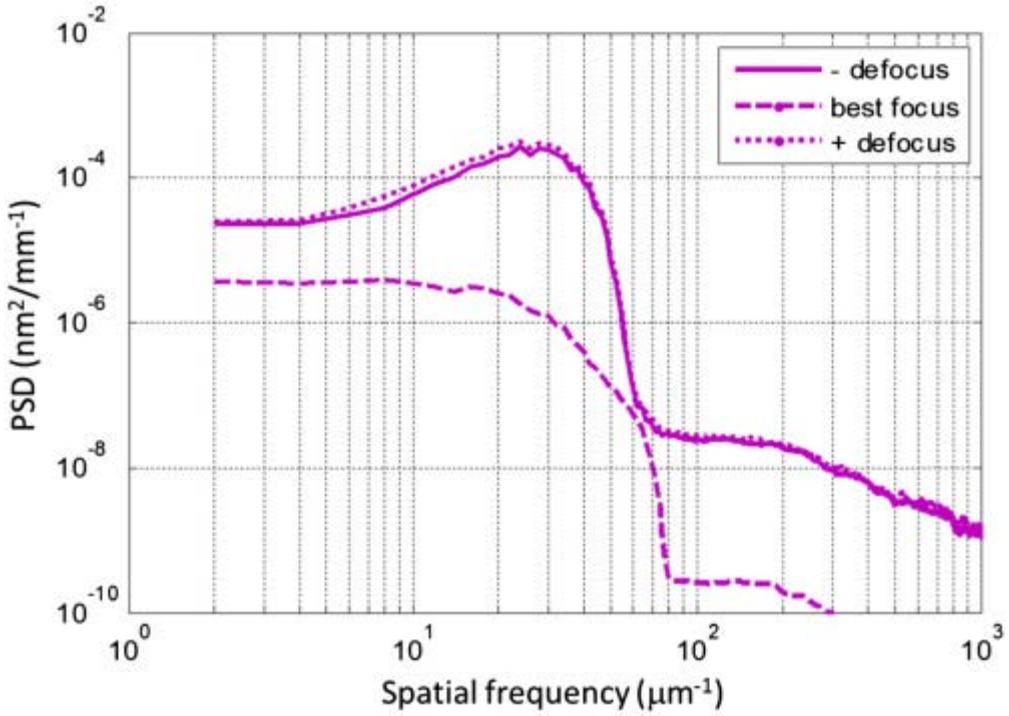

Fig. 14. LWR PSD for anamorphic case with 10-nm unshadowed lines and spaces at defocus values of 0 and ±0.6λ/NA2±0.6λ/NA2.

4. CONCLUSION

Hybrid thin mask/3D modeling has been used to study mask roughness effects in anamorphic 0.55-NA EUV lithography. Significant anisotropy is observed with shadowed lines showing substantially larger (approximately 2×2×) variability than unshadowed lines. Spectral analysis shows that the increased variability occurs primarily at the lower spatial frequencies. The spectral analysis also shows that despite the anamorphic imaging of isotropic mask roughness, the frequency cutoff in the image plane remains isotropic since it is determined by the isotropic image side NA. Finally, the analysis shows that for an assumed mask roughness of 67 pm, the relative LWR exceeds 10% at normalized defocus values exceeding 0.75. Achieving 0.55-NA performance equivalent to 0.33-NA performance in terms of fractional LWR would require the mask multilayer roughness to be improved by approximately 70%, i.e., reduced to better than 35 pm. The analysis performed here assumed a 70-nm-thick TaN absorber. To the extent to which the image line-edge slope is determined by the absorber properties, changing those properties will impact the resulting LER and LWR magnitudes. Going to a thinner and darker absorber, for example, with reduced 3D effects will result in reduced differences in horizontal and vertical variability performance.

Funding

This work was performed at Lawrence Berkeley National Laboratory (LBNL) with support from Intel Corporation; Samsung; EUV Tech; Inpria; JSR; U.S. Department of Energy (DOE) (DE-AC02-05CH11231).